Chapter 4

Spectroscopy of neon isotopes

4.1 Theoretical consideration

In this chapter the formation of *asymmetric molecular structures* in neon isotopes is discussed. The structure of some bands in ^{21}Ne can be interpreted as consisting of an intrinsic asymmetric structure (^{16}O+α) bound by a covalent neutron in σ and π orbitals. The observed parity doublet states in ^{21}Ne in the present experiment are discussed and a corresponding band structure for the states up to 12 MeV excitation energy in ^{21}Ne is given.

4.1.1 Cluster model

In the context of the covalently bound molecular structures in nuclei, the cluster structure of ^{21}Ne will be based on the underlying structure of ^{20}Ne. The cluster structure in ^{20}Ne has been discussed extensively in Refs. [But96, Ohk98, Kim01, Duf94]. In Ref. [Ohk98] it is shown that a shallow local potential, which is phase equivalent to the deep potential obtained in a double folding model [Abe93], gives an appropriate description of the scattering of α-particles on ^{16}O as well as explaining some some of the deformed rotational bands in ^{20}Ne [Ohk98, Abe93, Buc75]. The strong repulsion obtained in the potential at

small distances can be interpreted (similar to the case of the α+α system) as being due to the Pauli exclusion principle. Calculations based on the antisymmetrised molecular dynamics approach for ^{20}Ne performed by Horiuchi [Hor72, Kim01] also show the pronounced clustering. In the latter reference it is shown how the ^{16}O+α clustering related to the octupole degree of freedom, develops with increasing quadrupole deformation; the clustering appears for values of $\beta_2 \approx 0.32$.

4.1.2 Reflection asymmetric shapes

This approach was used to describe the structure of nuclei for the first time in the 1950's [Aza53, Ste54, Ste55] following the observation of low-lying negative parity states in actinide nuclei.

The origin of the octupole deformation can be understood from the single-particle level energy sequence for a harmonic-oscillator potential. In certain cases an orbit is lowered into the next lowest major shell by the l^2 and $l.s$ terms. These *intruder orbits* (l_{int}, j_{int}), lie close to orbits with $l = l_{int} - 3$ and $j = j_{int} - 3$, and the pairs of orbits with $\Delta l = \Delta j = 3$ can be strongly coupled by the octupole interaction.

Mean-field theories and algebraic models [But96] and macroscopic-microscopic methods [Lea75] suggest that reflection asymmetric shapes are observed in the lightest nuclei in the sd-shell and for even-even $N = Z$ nuclei, respectively. Experimentally this prediction can be supported by the observation of negative parity states in the middle of the sd-shell, where the shell model does not predict a large number of negative parity states [vO01, Des93]. These are typically intrinsic octupole shapes. The same observation of parity doublets is predicted for dinuclear systems (molecules) consisting of two clusters with unequal masses [Her50]. Such shapes, related to the observation of bands of opposite parity connected by strong $E1$ transitions, are well known in heavy odd mass nuclei.

Simplex quantum number

A reflection-symmetric nucleus has *Parity*, π, which describes the symmetry under space reflection , and *Signature*, σ, which describes the invariance with respect to a rotation of 180° about the rotation axis, which are good quantum numbers. For a reflection-asymmetric intrinsic structure the nucleus breaks the parity and signature symmetries, which means that both signature and parity are no longer good quantum numbers. The remaining symmetry is a combination of both and known as *simplex* [Goo74a, Naz85], which is still a good quantum number. The simplex is equivalent to a reflection in a symmetry plane (the plane containing the symmetry axis), and it is defined as the eigenvalues of the S operator

$$S = PR^{-1}. \tag{4.1}$$

In terms of simplex a rotational band having a simplex, s, has states of spin I with alternating parity, related by [Boh75],

$$p = se^{-i\pi I} \tag{4.2}$$

For a reflection asymmetric nucleus with even mass, the spin and parity sequences are restricted to

$$\begin{aligned} s = +1, \quad & I^\pi = 0^+, 1^-, 2^+, 3^-, ..., \\ s = -1, \quad & I^\pi = 0^-, 1^+, 2^-, 3^+, ..., \end{aligned} \tag{4.3}$$

and for the case of an odd mass nucleus

$$\begin{aligned} s = +i, \quad & I^\pi = \frac{1^+}{2}, \frac{3^-}{2}, \frac{5^+}{2}, \frac{7^-}{2}, ..., \\ s = -i, \quad & I^\pi = \frac{1^-}{2}, \frac{3^+}{2}, \frac{5^-}{2}, \frac{7^+}{2}, ..., \end{aligned} \tag{4.4}$$

Parity splitting

For the first time alternating-parity rotational bands with interleaved states in the sequence $I^+, (I+1)^-, (I+2)^+, ...$, were observed in the actinide region in ^{218}Ra and ^{222}Th [FN82, War83, Bon83], which were related to octupole deformation.

Figure 4.1 shows three different plots of potential energy, V, versus the octupole deformation, β_3. The top potential corresponds to a rigid spheroidal nucleus, which is axially symmetric as well as reflection symmetric in its ground state, but can undergo fluctuations (vibrations) about this symmetric shape. If the vibration is of odd multipolarity, then the nucleus can take on a reflection-asymmetric shape giving a $K^\pi = 1^-$ band at an energy of approximately 1MeV. The potential at the bottom of Fig. 4.1 represents a nucleus with a permanent ground state octupole deformation (*"a rigid pear shaped nucleus"*). The potential barrier has in this case two degenerate minima at $\pm\beta_3$ and rises to infinity at β_3=0. The nucleus can not take on a reflection-symmetric shape and the energy level spectra of such a nucleus with even mass is characterised by a set of perfectly interleaved state of alternating parity (*"parity inversion doublets"*). The case of the potential in the centre of Fig. 4.1 is intermediate between the two other potentials. There is a small potential barrier (see Fig. 4.1) and the nucleus can tunnel through the barrier to the mirror image shape. This interaction results in the displacement of the two bands. In reality, the limit shown by the bottom potential is not reachable, and the barrier separating the two degenerate minima is more like that pictured in the centre. The displacement of a state from the middle point of the two neighbouring states with opposite parity is known as the *parity splitting*, δE, and can be calculated by

$$\delta E = E(I)^- - \frac{1}{2}(E(I+1)^+ + E(I-1)^+). \tag{4.5}$$

In some nuclei it is observed that the parity splitting tends to zero at spins around $10\hbar$, giving energy level schemes similar to those shown in the lower part of Fig. 4.1. It seems that the rotation acts to stabilise the octupole deformation. Two possible explanations of this phenomena are: (i) the octupole shape has weaker pairing correlations, which increases the moment of inertia and (ii) the rotational motion perturbs the single-particle states of opposite parity, which brings the $\Delta l = \Delta j$=3 orbitals closer together, with increasing ro-

tational frequency, thereby enhancing the strength of the octupole correlations [Naz87, Egi90, Naz92].

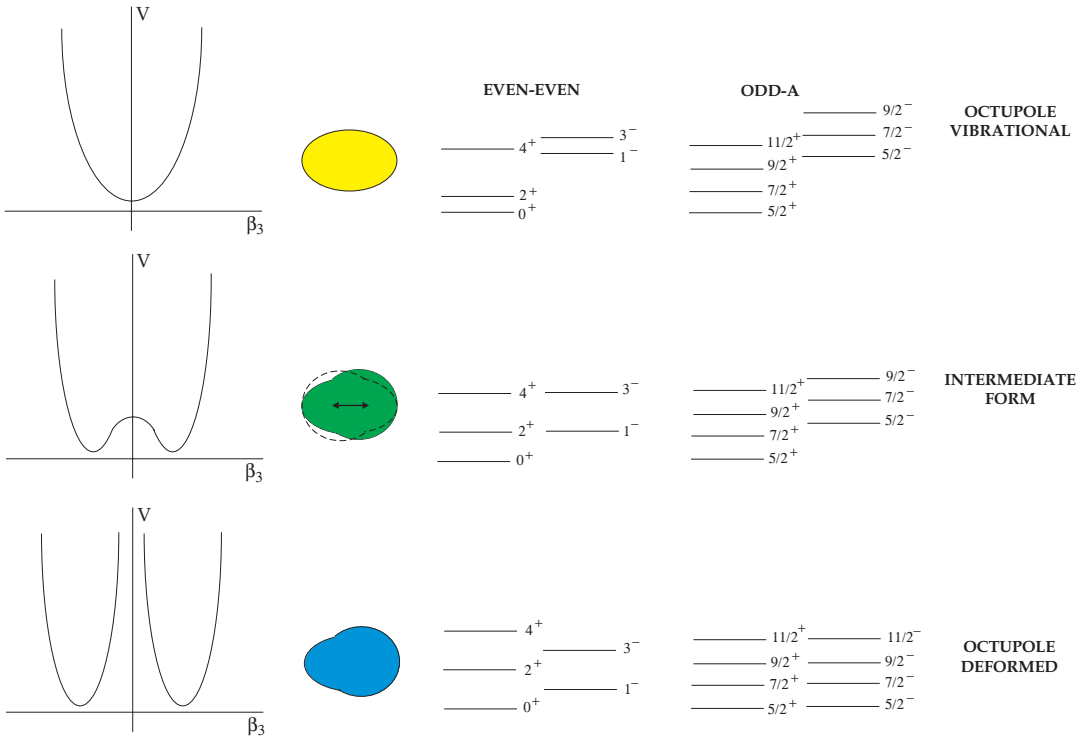

Figure 4.1: Plots of the potential energy and the associated energy level spectra for different axially symmetric (K=0) shapes with octupole deformation. The top potential represents a nucleus with reflection-symmetric ground state shape. The centre potential is an intermediate case between this form and the static octupole-deformed shape, which corresponds to the bottom potential.

In odd nuclei reflection asymmetric shapes are manifested through the appearance of doublets of states with opposite parities with an energy splitting depending on the height of the internal barrier separating the two reflected configurations. Such intrinsic parity-violating shapes, related to bands of opposite parity, for example for ^{19}F and ^{21}Ne, have also been interpreted as possible evidence for cluster and molecular structures [vO01, Des93]. The energy surface can have two minima in the octupole degree of freedom. This is schematically

illustrated in Fig. 4.2, where two shapes with $\beta_3 < 0$ and $\beta_3 > 0$ are separated by a potential barrier. A rearrangement of nucleons, or a tunneling process by the nucleons, will bring the system from the state with $\beta_3 > 0$ to the other shape, the reflected configuration with $\beta_3 < 0$.

A particularly interesting case which has recently been discussed in the context of the clustering or octupole scenario, is the nucleus ^{21}Ne [vO01]. As for the case of ^{20}Ne, the inverted doublet structure which, based on the α + ^{16}O, has been discussed in 1972 by Horiuchi *et al.* [Hor72].

In ^{21}Ne this parity doublet structure is mirrored in two parity doublets of bands with $K = 3/2$ and $K = 1/2$. Although mixing of the corresponding positive parity states with states of quadrupole deformation is to be expected, the negative parity states are difficult to relate to simple Nilsson orbitals, suggesting an interpretation based on cluster configurations. In most papers on the structure of light sd-shell nuclei the negative parity states have been omitted in the discussion of the level structure *e.g.* Refs. [Hof89, Jia92], because they invoke complicated particle excitations to the p-shell as well as to the f-shell.

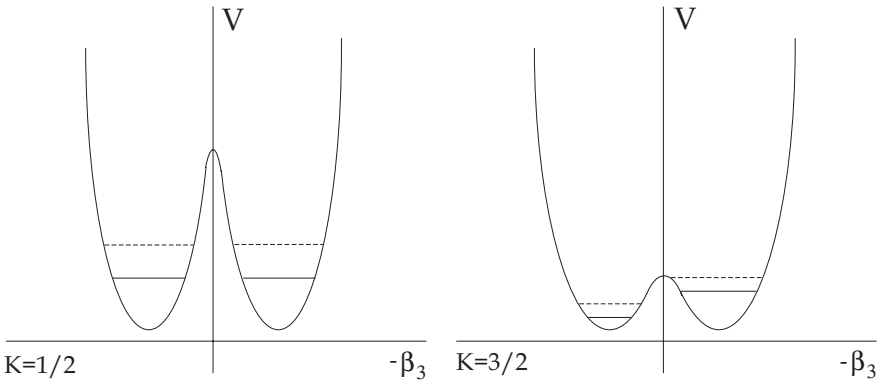

Figure 4.2: The potential $V(\beta_3, I)$ for fixed angular momentum, I, as a function of β_3 showing the two symmetric minima in the proposed bands in ^{21}Na. For the $K = 3/2$ bands the lower barrier induces a large energy splitting; for $K = 1/2$ the higher internal barrier gives degenerate positive and negative parity bands.

The ground state structure of ^{21}Ne has been described in cluster calculations using the microscopic three-cluster generator coordinate method [Des93].

One of the descriptions is based on the mixing of different ^{16}O+α+n configurations, which give rise to an intrinsic reflection asymmetric shape, whereas in others a reflection symmetric shape of the α+^{12}C+α+n structure is preferred.

Having in mind the γ-decay properties connected to reflection asymmetric (octupole) shapes, we have investigated the rotational structure of ^{21}Ne and ^{21}Na. The result is that the excited states of ^{21}Ne are consistent with the formation of a molecular structure with a stable dipole moment. An estimate of the intrinsic dipole moment based on γ-ray branches gives a limiting value in agreement with an intrinsic ^{16}O+^{4}He+n configuration.

Octupole bands in ^{20}Ne and ^{21}Ne

The structure of ^{20}Ne has also been discussed within the framework of the deformed Nilsson model suggesting stable quadrupole and octupole deformations [But96, Buc75]. Similarly, rotational bands as parity doublets using cluster models and octupole shapes have been obtained in other light nuclei such as ^{18}O [Rei93] and ^{19}F [Kra69, Duf94].

Experimentally, two opposite parity bands are observed in ^{20}Ne: the negative parity band starting with a 1^- state at 5.787 MeV, and the positive parity band being the ground-state band. This observed structure supports the identification of the two bands as 'inversion doublets' of an intrinsic reflection asymmetric octupole with $K = 0$ and parities $\pi = (+ \text{ and } -)$; the energy splitting between the two bands is approximately 5 MeV. Further states in higher lying bands in ^{20}Ne of positive and negative parity are obtained using the α + ^{16}O model by Ohkubo *et al.* [Ohk98].

For ^{21}Ne this concept of octupole deformation and a weak coupling of the cluster shape with an extra valence neutron leads to a close analogy to spin parity doublets with $K = 3/2$ and $K = 1/2$. Such 'parity doublets', in the context of a

reflection asymmetric molecular structure and one covalent molecular orbital for neutrons, are discussed in Ref. [vO01].

4.2 Experiments: ^{18}O+^{13}C and ^{7}Li+^{16}O reactions

In the present experiment excited states of ^{21}Ne and ^{21}Na have been populated in the ^{7}Li + ^{16}O reaction from the ^{7}Li + ^{10}BeO experiment, described in Section 3.3.

Since the performed experiment was optimised to investigate γ-ray transitions in isotopes of Be, B and C, and the energy was chosen to be below the Coulomb barrier on the nuclei in the backing to avoid reactions, only low angular momenta states were populated. In Fig. 4.3 are shown all γ-ray transitions in ^{21}Ne from states populated in the ^{7}Li+^{16}O reaction.

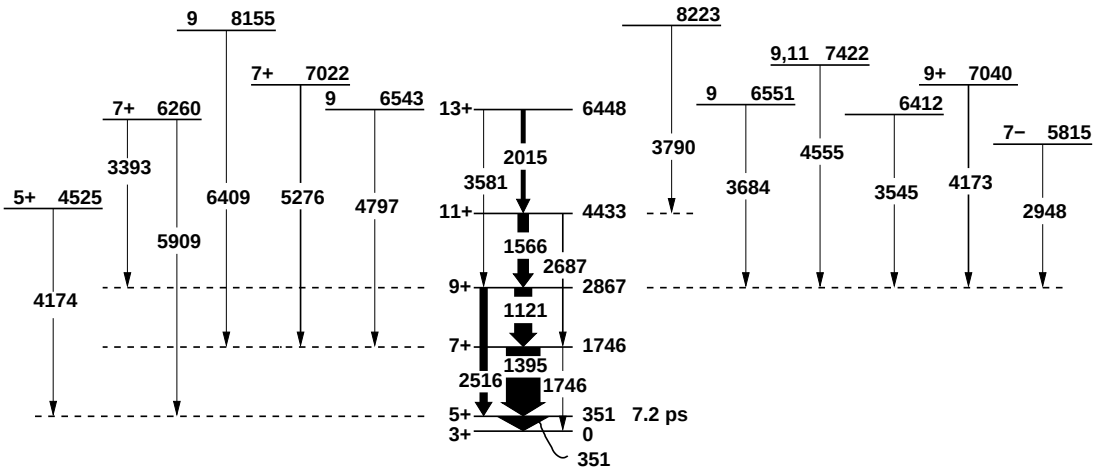

Figure 4.3: Decay scheme of ^{21}Ne showing the levels not forming rotational structures together with the $K^\pi = 3/2^+$ ground-state band as observed in the present work. All energies are given in keV. The intensities (widths) of the arrows are not to scale, except for the $K^\pi = 3/2^+$ band.

Meanwhile, another experiment discussed in this work was performed with the reaction ^{13}C(^{18}O, $2\alpha 2n$)^{21}Ne at a beam energy of 100 MeV in order to enhance the population of higher spin levels in particular the $K = 1/2$ band members.

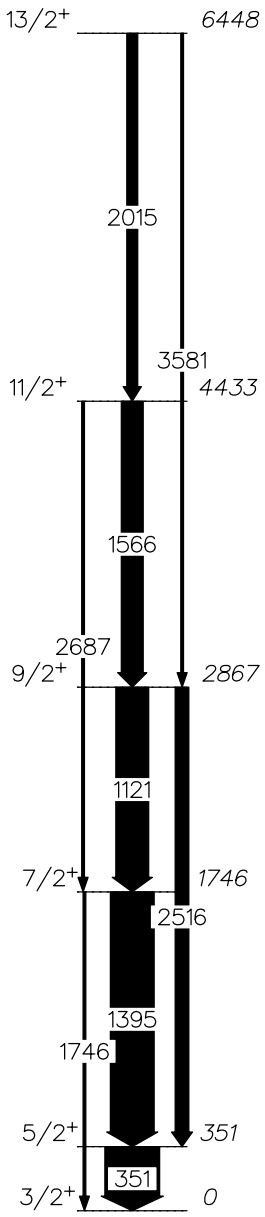

Figure 4.4: Gamma-ray decay scheme for ^{21}Ne as observed in the ^{18}O+^{13}C reaction. All energies are given in keV.

In this purely compound nucleus reaction only yrast and nearly yrast states are strongly populated (see Fig. 4.4).

The results obtained for the yrast band decay from this experiment, which are shown in Fig. 4.4 are in good agreement with the results from the first ^{7}Li+^{16}O experiment.

4.3 Results and discussion

4.3.1 Octupole bands in ^{21}Ne

To underline the proposed rotational character of bands in ^{21}Ne, excited states from previous work and the newly observed states in this work have been arranged into rotational-like structures with K values of 1/2 and 3/2. In Fig. 4.5 are shown the pairs of opposite parity states of the proposed octupole configurations arranged in parity doublets (see details in Ref. [vO01]). For the K=1/2 bands the higher lying states are slightly different from Ref. [vO01].

In Fig. 4.5, additional levels associated with structures corresponding to the 'normal' quadrupole-deformation are not included. These have been discussed in previous studies, which have established the main features of the γ-decay in this nucleus [Hof89, Rol71, Rol72, Kuh74, War71, And81, Pil72].

The most striking characteristic for the K=1/2 bands, besides the small energy splitting of the parity doublets, is the long lifetime (110 ps) of the $1/2^-$ state at 2.79 MeV decaying into the $K = 3/2$ ground state band.

In the cluster description this requires a re-arrangement from a π-type neutron orbital (see Section 3.1.2.) with densities outside the symmetry axis to a σ-type bond [vO01], where neutrons are concentrated along the symmetry axis.

With a lifetime of 110 ps the competing M2 and E1 transitions connecting the $1/2^-$ state to the $5/2^+$ and the $3/2^+$ states of the $K = 3/2$ ground-state band respectively, thus appear to be retarded by more than three orders of mag-

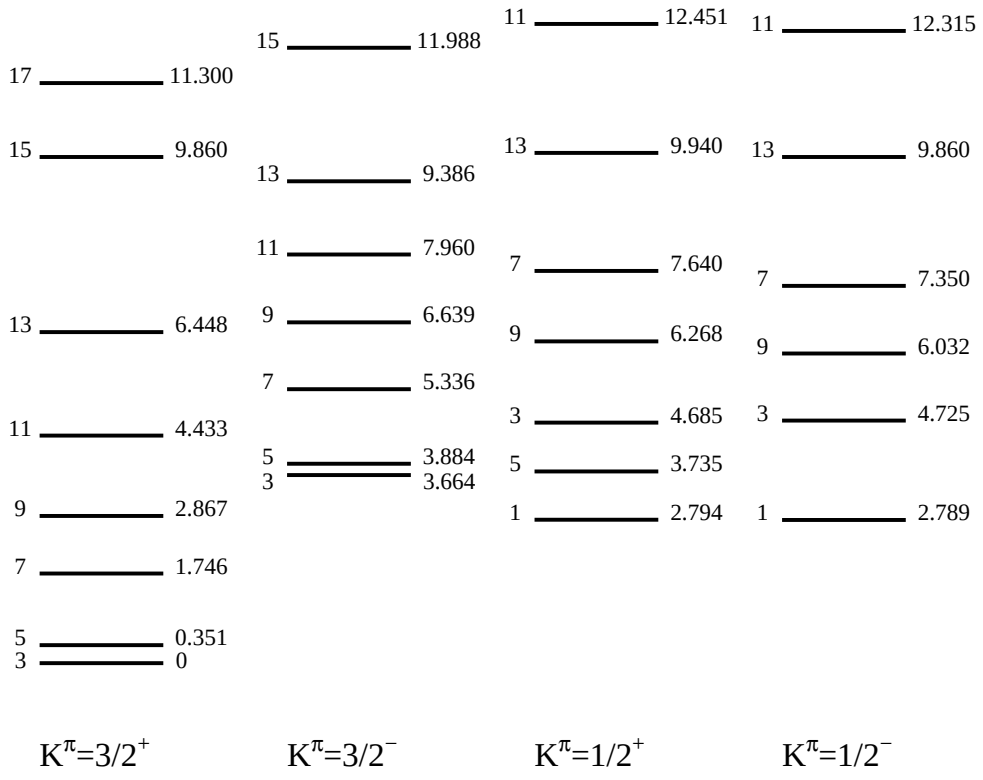

Figure 4.5: Rotational band structure of ^{21}Ne proposed here, showing the parity doublet structure (based on Fig. 4 of Ref. [vO01]). All energies are given in keV. The parity of the states follow the band assignments.

nitude. The intensity ratio from the presented experimental data for the two transitions with 2789 keV (E1) and 2438 keV (M2) is E1/M2 = 3. Warburton *et al.* [War71] have measured this ratio and obtained a value of 5.7. Using the common systematics of the relative strength of E1 and M2 transitions, the E1 transition would be expected to be stronger than the M2 transition by a factor of 10^6. Whereas in the data presented here it is stronger only by a factor of 3. The strong suppression of the E1 transition once more indicates that the configurations are not related to single centre (mean-field) structures, but to two centre molecular configurations. Two possible explanations were already discussed in Ref. [War71]. The explanation of this fact, which is discussed in this work, is that

the enhanced de-excitation through an M2 transition is related to the change of two quantum numbers going from the $1/2^-$ state ($K^\pi = 1/2^-$ band) to the $5/2^+$ or to the $3/2^+$ state ($K^\pi = 3/2^+$ band), namely the change of the orbital angular momentum and the relative spin orientation, in order to change the K-value. The almost degenerate $I^\pi = 1/2^+$ and $1/2^-$ levels and consequently the small energy splitting in the $K = 1/2$ bands suggests that the internal energy barrier between $\beta_3 < 0$ and $\beta_3 > 0$ for such a change of configuration is quite high (see Fig. 4.2).

In Fig. 4.8 the observed transitions between states of the proposed octupole character are shown in the newly ordered band structure. Fig. 4.6 shows the remaining transitions observed in the ^{7}Li + ^{16}O experiment, together with the ground-state band, namely the part of the level scheme of ^{21}Ne which does not seem to be connected to the band structures discussed above.

The $K^\pi = 3/2^+$ ground-state band has been observed with intraband transitions up to the $I^\pi = 13/2^+$ state at an excitation energy of 6448 keV. The states in the $K^\pi = 3/2^-$ band have been identified through their *interband* decays to the $K^\pi = 3/2^+$ band. No *intraband* γ-transitions have been observed in the negative parity band. The lowest state in this band ($3/2^-$, 3664 keV) also feeds the $1/2^-$ state of the $K^\pi = 1/2^-$ band, with an intensity, a factor of three lower when compared to its transition to the $K^\pi = 3/2^+$ band. The fact that the members of the $K^\pi = 3/2^-$ band decay predominantly into states of the $K^\pi = 3/2^+$ band is consistent with the fact that we are dealing with strongly enhanced E1 transitions. The existence of an E1 transition connecting the I^π=$3/2^-$ bandhead to the ground state could not be clearly established due to the absence of a feeding transition on which to gate and due to the poor selectivity of the ungated spectra.

The transitions de-populating the states differing by intervals of 2 units of spin from the $K = 3/2$ bandhead, namely $J^\pi = 3/2^-$, $7/2^-$, $11/2^-$, $15/2^-$, are clearly visible (see Fig. 4.8), whereas the transitions de-populating the interleaved $5/2^-$, $9/2^-$ states (and the unobserved $13/2^-$) are much weaker. The $13/2^- \rightarrow 11/2^+$ transition could not be observed in the present data. This is probably due to

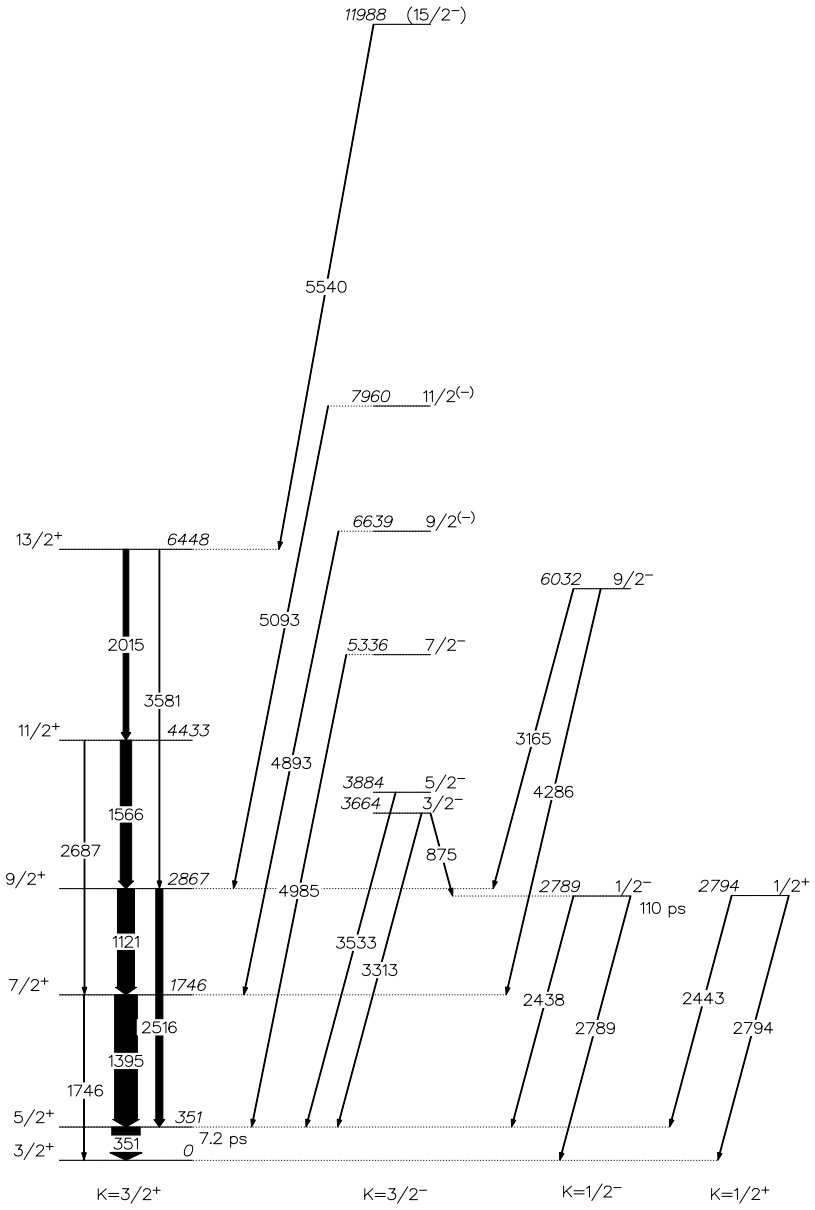

Figure 4.6: Gamma-ray decays observed in the ^{16}O(^{7}Li,np) reaction showing the proposed $K = 3/2$ and $K = 1/2$ bands of ^{21}Ne. All energies are given in keV. The intensities (widths) of arrows to the right side of the ground-state band are not to scale.

the rather low γ-ray branch in this region of excitation energy ($E_x > 9\,\mathrm{MeV}$), as it is inferred from very low Γ_γ/Γ-values measured by Billowes *et al.* [Bil87]. (The only exception is the $15/2^-$ level at 11.988 MeV excitation energy.) The $5/2^- \rightarrow 5/2^+$, 3533 keV transition could not be confirmed because of its partial overlap with the 3545 keV γ-ray transition de-exciting the state at 6412 keV (see Fig. 4.8).

The *non-observation of the intraband E2 transitions* allows an estimate to be made of the ratio of the observed $B(E1)/B(E2)$ branching ratios. The intrinsic dipole moment is related to the $E1$ transition probability by the rotational model formula (see section 3.1.3)

$$B(E1, I_i \rightarrow I_f) = \frac{3}{4\pi} e^2 D_0^2 |\langle I_i K_i 10 | I_f K_f \rangle|^2, \tag{4.6}$$

and the $E2$ transition probability to the quadrupole moment by

$$B(E2, I_i \rightarrow I_f) = \frac{5}{16\pi} e^2 Q_0^2 |\langle I_i K_i 20 | I_f K_f \rangle|^2. \tag{4.7}$$

These formulae provide a consistent method to extract the intrinsic dipole moments from the experimental data, although the assumption that the investigated nucleus is a good rotor may be questionable. The experimentally measured intrinsic dipole moments in several regions of the nuclear chart can be found in the review article of Butler and Nazarewicz [But96].

Assuming for ^{21}Ne, that the same value of the measured intrinsic quadrupole moment of ^{20}Ne occurs, namely, Q_0= 58(3) $e.fm^2$ [Hor71], the intrinsic dipole moment for ^{21}Ne is expected to be $D_0 > 0.1$ $e.fm$. This large value for D_0 is indicative of stable octupole deformation, as expected for a reflection asymmetric ^{16}O+α+n structure.

The $K^\pi = 1/2^+$ band was visible in the data only by its weak transitions from the bandhead to the lowest states ($3/2^+$ and $5/2^+$) in the $K^\pi = 3/2^+$ band. No feeding of the $K = 1/2^+$ bandhead by γ-ray decays from other members of this band could be identified, although its decay is observed.

The de-population of the 6032 keV $9/2^-$ state, which is proposed to be a member of the $K = 1/2^-$ band, into the $9/2^+$ and $7/2^+$ levels of the $K = 3/2^+$ band has also been observed. Some mixing between the state of the $K = 3/2^-$ band at 6639 keV excitation energy and the $K = 1/2^-$ band member at 6039 keV, both with spin $9/2^-$, cannot be excluded.

For the $K^\pi = 1/2^-$ bandhead, fed by the $J^\pi = 3/2^-$ ($K = 3/2^-$) state, transitions de-populating the $1/2^-$ level were observed. Further feeding of the bandhead was not observed. From this observation and the absence of γ-ray feeding of the $K = 3/2^-$ band and the $K = 1/2^+$ bandhead, a conclusion could be made, that the population patterns observed in this experiment, give very strong indications for the direct population of these states. This direct population must originate from an α-transfer followed by the transfer of a neutron, leaving two nucleons (a neutron and proton) to be emitted in a direct process.

The population of the low-spin states of the $K = 1/2$ bands is remarkable and indicates the formation of cluster states, because the (^7Li, np) or (^7Li, d) reactions favour states with higher spin, due to the angular momentum mismatch between incoming and outgoing channels. A similarly strong population of cluster states via ^{5}He has been observed in ^{14}C in a recent study of the ^{9}Be(^{7}Li, d)^{14}C reaction using a high resolution Q3D-spectrometer [Boh02].

4.3.2 Angular distributions and DCO ratios

A nucleus formed in a fusion-evaporation reaction is in a state with its angular momentum vector perpendicular to the axis of the beam direction. Even after the subsequent evaporation of particles the residual nucleus keeps a high degree of orientation for a long time (of the order of nanoseconds). If γ rays are emitted from a nucleus in such a state, the angular distribution of the relative intensities (with respect to the beam axis) depends on the multipolarity of the transitions. This distribution [Sie65] is given by the equation:

$$I(\theta) = \sum_{\ell=even} A_\ell P_\ell(\cos\theta) \tag{4.8}$$

where $P_\ell(\cos\theta)$ are the Legendre polynomials and A_ℓ are their coefficients. The coefficients are tabulated (see, for example, Ref. [dM74]).

Figure 4.7 shows the angular distributions for pure quadrupole and dipole transitions. By examining the relative γ-ray coincidence intensities at angles approximating 0° (for example) and 90° it is possible for different multipoles to be distinguished. This method is called Directional Correlations de-exciting Oriented states (DCO) [Kra73].

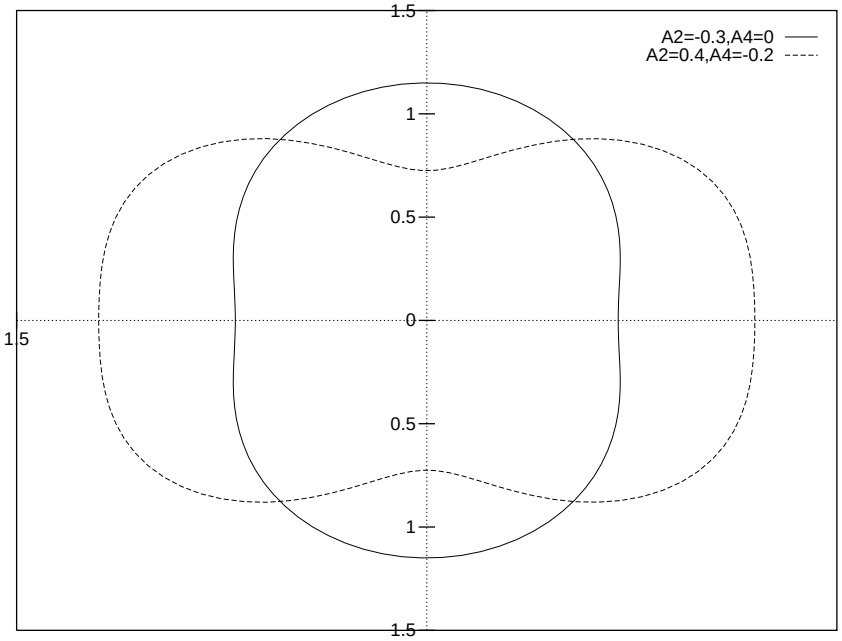

Figure 4.7: Intensity distributions for a dipole (ΔI=1) transition (solid line) and a quadrupole (ΔI=2) transition (dashed line) as a function of the angle θ, with respect to the beam direction. (Zero degrees corresponds to the positive x-axis.)

The spins and parities of the ^{21}Ne levels were deduced, where possible, using the DCO analysis. Special attention was paid to the DCO ratio for charged particle coincidence events. For the data obtained with the GASP detector array (see Chapter 2) a γ–γ matrix was created with γ rays from the germanium detectors at

90° with respect to the beam direction on one axis and the γ rays from those detectors at 34° and 146° on the second axis. In order to reduce contamination from other reaction channels the data in the matrix have been sorted under the condition of being in coincidence with 0 and 1 proton detected in the ISIS Si-telescopes. Gates were set on both axes on known stretched quadrupole E2 transitions and the intensities of the transitions of interest were extracted from the resulting spectra. The theoretical DCO ratios, $R_{DCO} = I_\gamma(90°)/I_\gamma(34°)$, in the GASP geometry are R_{DCO} ≈1.0 for stretched quadrupole (E2), and R_{DCO} ≈2.0 for pure dipole (E1 or M1) transitions. However, if the gates are set on a pure dipole transition, the expected DCO ratios for quadrupole and for dipole transitions are ≈0.5 and ≈1.0, respectively. Table 4.1 shows the results of the DCO analysis for the transitions, where the analysis was possible. Most of the published spin assignments could be confirmed. The cases where a new spin assignment is possible, are marked with (*).

In Table 4.2 the new spin assignments obtained from the experimental data are listed. The assignment of the 7040 keV and 7422 keV need to be confirmed. In the recent Nuclear Data Tables [htt02], a state at 6552 keV, de-populating via a 4806 keV γ ray to the 1746 keV, $7/2^+$ state, is published. It is possible that this is the same state as at 6543 keV with here the same transition as the 4797 keV γ-ray.

4.3.3 The mirror nuclei ^{21}Ne and ^{21}Na

The background subtracted spectra relevant for the γ-ray decays observed in ^{21}Na and ^{21}Ne are shown in Figs. 4.8 and 4.9, both gated on the lowest $5/2^+ \rightarrow 3/2^+$ (g.s.) transition in the respective nuclei. The Doppler-shift correction has been done by an optimisation procedure of the recoil velocity since the lifetimes of the states, except for the long-lived $5/2^+$ and $1/2^-$ levels at 351 keV and 2789 keV respectively, in ^{21}Ne, and the $5/2^+$ level at 332 keV in ^{21}Na, were shorter than

$\mathbf{E}_\gamma$ [keV]	$\mathbf{J}_i^\pi \rightarrow \mathbf{J}_f^\pi$	R_{DCO}
1121	$9/2^+ \rightarrow 7/2^+$	1.00 ± 0.01
1395	$7/2^+ \rightarrow 5/2^+$	1.10 ± 0.01
1566	$11/2^+ \rightarrow 9/2^+$	1.06 ± 0.02
2687	$11/2^+ \rightarrow 7/2^+$	0.50 ± 0.02
3165	$(9/2^-) \rightarrow 9/2^+$	0.67 ± 0.05
4173*	$9/2^+ \rightarrow 9/2^+$	0.74 ± 0.06
	$5/2^+ \rightarrow 5/2^+$	
4286	$9/2^- \rightarrow 7/2^+$	1.05 ± 0.04
4555*	$9/2, 11/2 \rightarrow 9/2^+$	0.69 ± 0.02
4797*	$9/2 \rightarrow 7/2^+$	1.29 ± 0.11
4985	$7/2^- \rightarrow 5/2^+$	0.86 ± 0.08
5093*	$11/2^{(-)} \rightarrow 9/2^+$	1.04 ± 0.08

Table 4.1: DCO ratios for transitions in ^{21}Ne, gated by the $5/2^+ \rightarrow 3/2^+$ transition at 351 keV.

E [keV]	$\mathbf{J}^\pi$ (this work)	$\mathbf{J}^\pi$ (former assignment [htt02])
6543	$9/2$	(see text)
7040	$9/2^+$	$(5/2, 9/2^+)$
7422	$9/2, 11/2$	$(7/2^+, 11/2^-)$
7960	$11/2^{(-)}$	(new state)

Table 4.2: Newly derived spin assignments obtained from the recent experiment as deduced from the DCO ratios (marked with (*) in Table 4.1). The third column shows the assignments before this work.

the stopping time of the nuclei in the backing material.

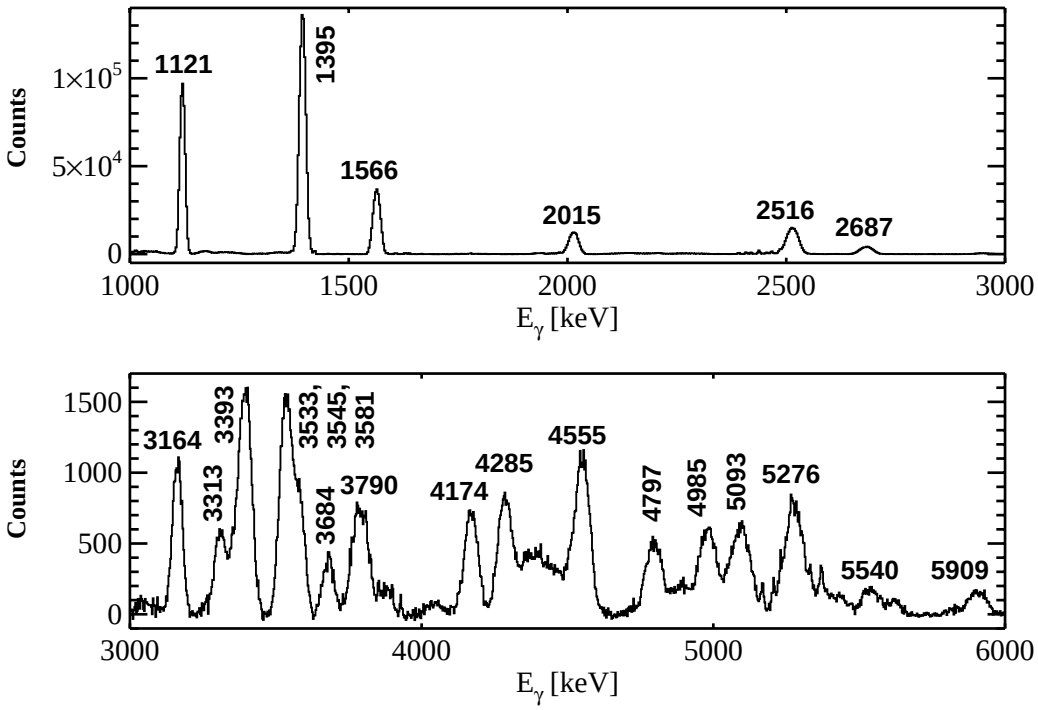

Figure 4.8: Gamma-ray spectrum obtained by gating on the 351 keV ($5/2^+ \rightarrow 3/2^+$) ground-state band transition in ^{21}Ne. The labelled peaks are all placed in ^{21}Ne.

For ^{21}Na no peaks have been observed above 3 MeV. Comparing the peak intensities of ^{21}Ne and ^{21}Na in the energy region between 1 and 3 MeV and the peak strengths of ^{21}Ne in the energy region above 3 MeV, peaks of ^{21}Na (if existing) with a few tens of counts would be expected. Since there are no peaks observed above 3 MeV when gating on the lowest lying transition in ^{21}Na, it is likely that there are no transitions from states populated in ^{21}Na above 3 MeV in the present reaction in coincidence with the $5/2^+ \rightarrow 3/2^+$ transition.

The nucleus ^{21}Na is populated via the $(^7Li, 2n)$ reaction. Fig. 4.10 shows the level scheme and γ-ray decay pattern of ^{21}Na as observed in the present experiment. Two new transitions have been added to the previously known level

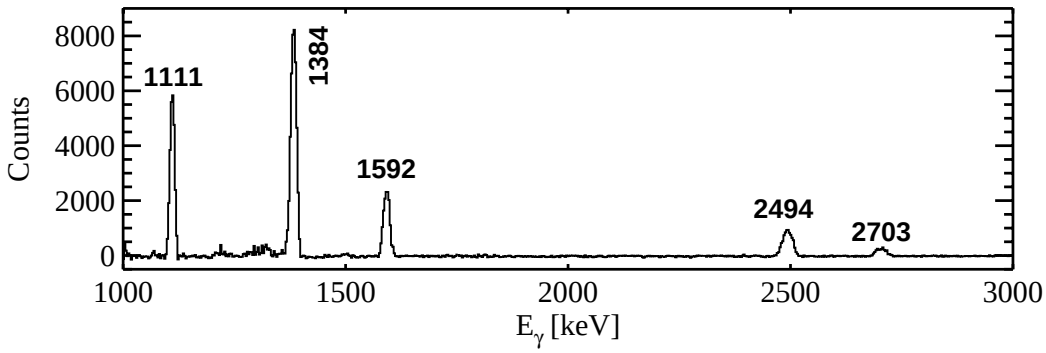

Figure 4.9: Gamma-ray spectrum obtained by gating on the 332 keV ($5/2^+ \rightarrow 3/2^+$) ground-state band transition in ^{21}Na. All labelled peaks belong to ^{21}Na and no peaks are observed above 3 MeV.

scheme extending the ground-state ($K^\pi = 3/2^+$) band up to a state at 4419 keV for which an I^π=$11/2^+$ assignment is proposed.

Since both ^{21}Ne and ^{21}Na are mirror nuclei, *i.e.* the neutron number of one equals the proton number of the other and vice versa, it can be seen by comparison of the two nuclei that the nuclear structure is very similar. This is a consequence of the fact that the nuclear force does not distinguish between neutrons and protons. Conversely, the existence of an additional proton, *i.e.* an additional charge, in one of the mirror nuclei (^{21}Na) causes a difference in the energy of the isobaric analogue states due to the Coulomb interaction.

Recently, the Coulomb energy difference (CED), the energy difference between isobaric analogue states defined as $CED = E^*(^{21}Na) - E^*(^{21}Ne)$, has been investigated in a series of mirror nuclei in the $f_{7/2}$ shell, allowing the study of the spatial behaviour of the wave functions of the active valence nucleons [Ben98, Ekm00, Len01]. Since the Coulomb energy is only due to protons, it has been pointed out that when a $J = 0$ proton pair (of the core) couples to another J-configuration, the Coulomb energy decreases [Ben98]. In the $J = 0$ coupling the overlap of the two proton wave function (and therefore the Coulomb repulsion) is

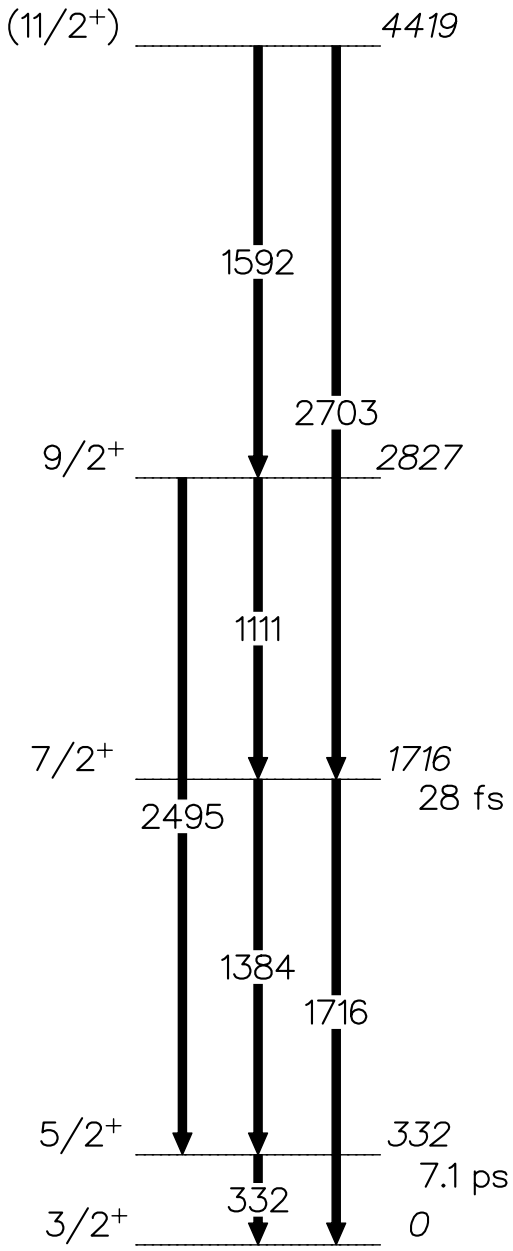

Figure 4.10: Scheme showing the ground-state band and γ-ray transitions of ^{21}Na as obtained in the present work. All energies are given in keV.

at a maximum. Moreover the detailed behaviour of the CED has been proven to be sensitive to the changes in the radii of the valence particles in different excited states [Len01].

Fig. 4.11 shows the CED for the $K^\pi = 3/2^+$ bands in ^{21}Ne and ^{21}Na from the present data. A decrease of the CED as function of spin up to I=9/2 $\hbar$, followed by an increase when approaching the maximum alignment of two particles in the $d_{5/2}$ orbit, was observed. The qualitative behaviour of the CED here is consistent with the result of antisymmetrised molecular dynamics calculations for ^{20}Ne, where at higher spin the charge density becomes more compact.

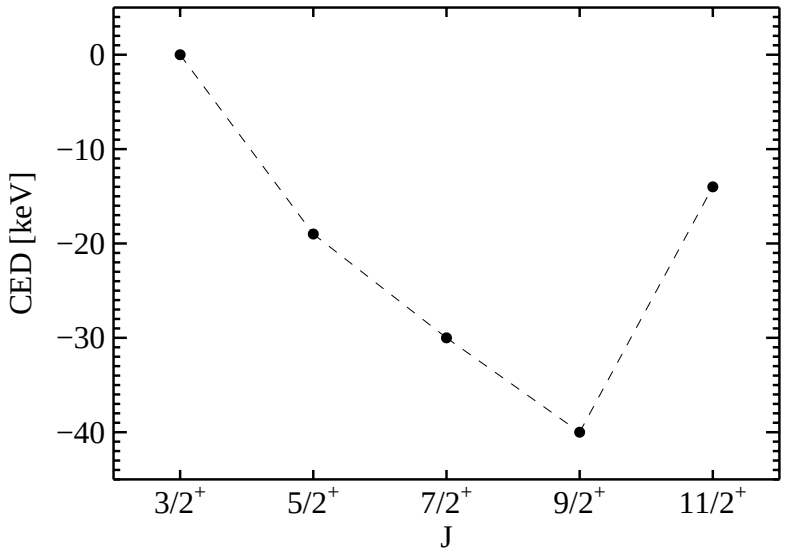

Figure 4.11: Coulomb Energy Difference (CED) between mirror states for the $K^\pi = 3/2^+$ band in ^{21}Na and ^{21}Ne (see text for details).

The antisymmetrised molecular dynamics calculations by Kanada-En'yo *et al.* and Horiuchi *et al.* [KE95b, Hor95] predict a shrinking of the average radius of the core-cluster with increasing angular momentum. This shrinking of the radius in the α + ^{16}O-system with spin, is also suggested by the result for the α + ^{16}O potential of Ref. [Ohk98], where the potential minimum moves to smaller distances for larger L-values (see also Section 2.1 of Ref. [vO01]).

Taking into account the above mentioned mass distribution of the valence particles, it is likely that for the $K = 3/2$ configuration a covalent orbit of the π-type involves a proton or neutron distribution concentrated outside the symmetry axis. A shrinking of the core extension translates to an increased Coulomb repulsion for the covalently bound proton and corresponds to a decrease in the CED.

4.3.4 Gamma-ray decays and band structure in ^{22,23}Ne

^{22}Ne

In this even-even nucleus, as can be seen from the Nilsson diagram (see Fig. 1.5) all nucleons are coupled and the spin of the ground state is 0^+. In the ^{18}O+^{13}C reaction studied here the ground-state band ($K^\pi = 0^+$) was strongly populated and 3 new γ-ray transitions and 2 new levels were found. The ground-state band was extended to higher spin (8^+). In Fig. 4.12 the γ-ray transitions in coincidence with the new transition from the 8^+ level at 11030 keV excitation energy are shown. A level at 11032 keV excitation energy was measured in an ^{18}O(α,γ) [htt02] reaction. In Fig. 4.13 excitation energy versus J(J+1) is plotted which shows that this nucleus is a very good rotor.

In this reaction as can be seen from Fig. 4.14 showing all γ-ray transitions gated by the decay to the ground state at 1274 keV, the rest of the populated states are likely to be intrinsic, based on single-particle excitations or rotational levels from other band structures.

Fitting the experimental data for the energy levels it is possible to obtain the rotational constant α, which is connected with the moment of inertia Θ ($\alpha = \hbar/2\Theta$). The value obtained is 140 keV.

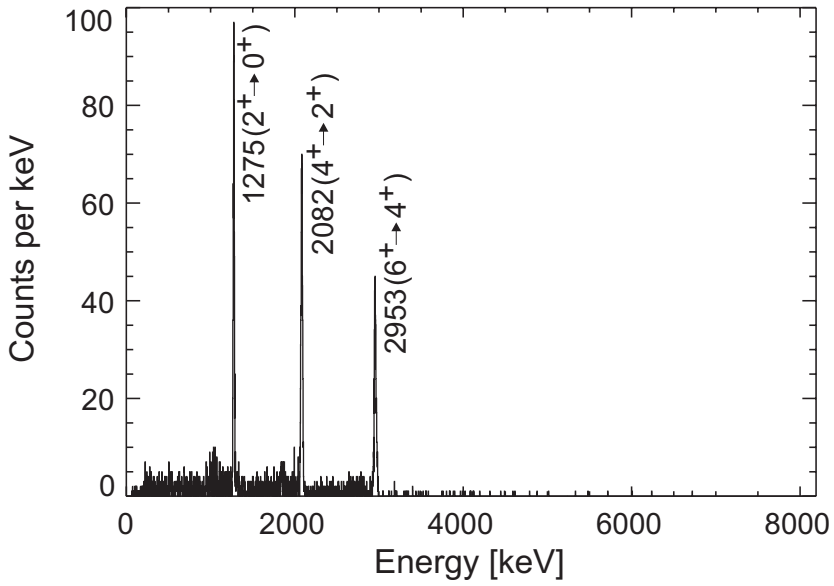

Figure 4.12: Gamma-decay spectrum gated by the new 4719 keV ($8^+ \rightarrow 6^+$) transition in the $K = 0^+$ ground-state band in ^{22}Ne.

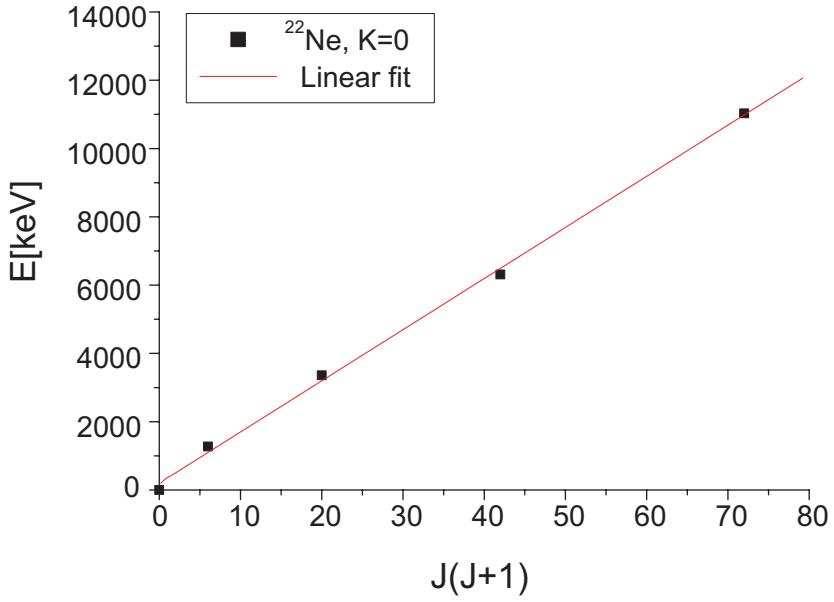

Figure 4.13: Excitation energy versus J(J+1) plot for the positive parity yrast band in ^{22}Ne as obtained from the current data.

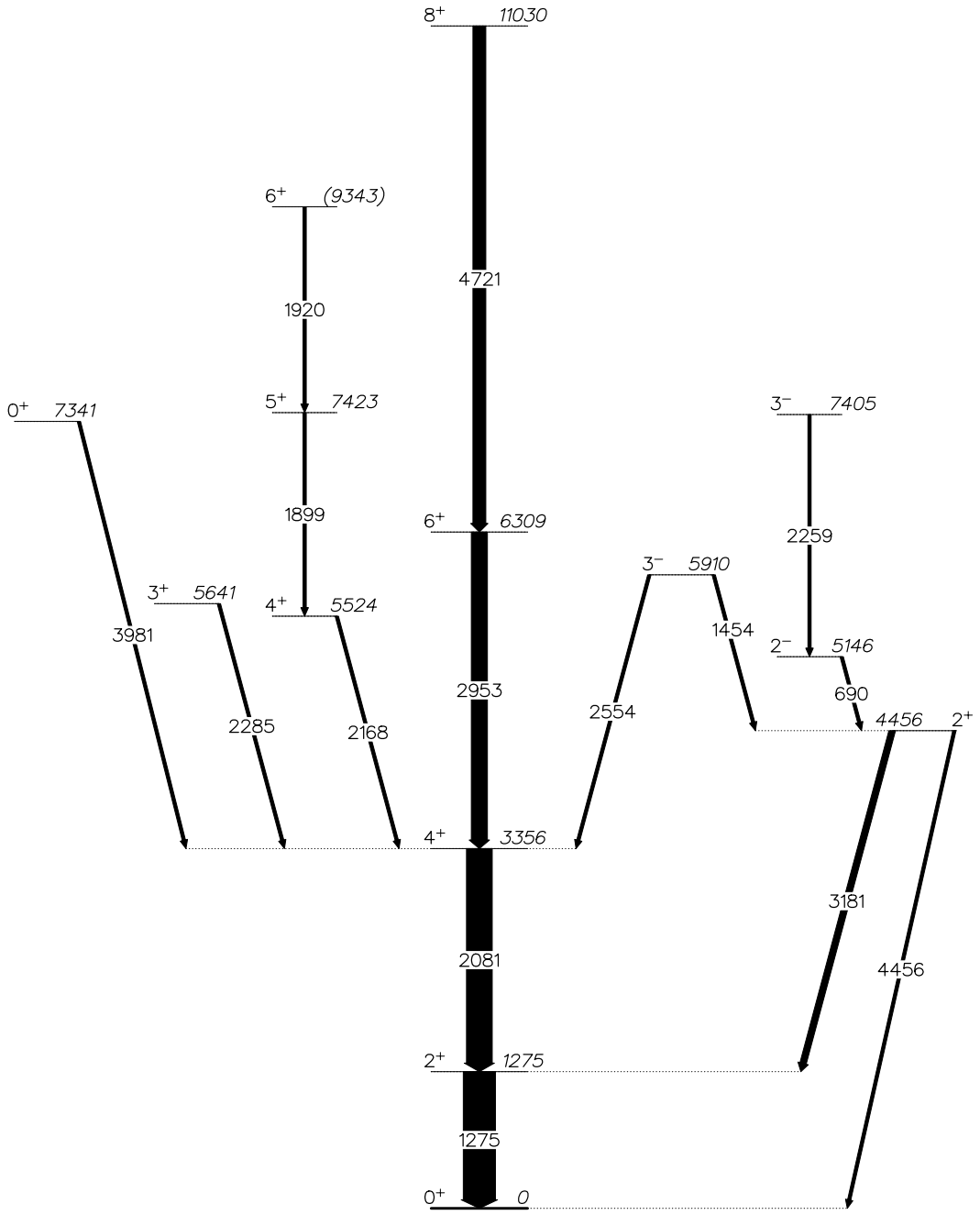

Figure 4.14: Gamma-ray decay scheme for ^{22}Ne as observed in this experiment. Energies are in keV.

^{23}Ne: deformation alignment

The mechanism of deformation alignment is capable of producing high-K rotational bands with either yrast status, as in the case presented in this work, or at marginally higher excitation energy in almost all deformed *sd* shell nuclei with an approximate balance between the number of protons and neutrons. The only exceptions are observed for A=19-22.

The theoretical prediction [Roe00] (see Fig. 4.15) for the low-lying $K^{\pi}=5/2^{+}$ rotational band is based on the deformation-aligned multi-particle configurations of the Nilsson-model. The band is based on the $(3/2)^2(5/2)^1$ configuration. The theoretically predicted members of the band lie at E_x= 0, 1702, 2517, 3931*, 5926* keV where the last two levels are from shell-model calculations. The members of the band as observed in the ^{13}C(^{18}O, 2α)^{23}Ne reaction are shown in Fig. 4.15 and 4.16. The level at 3843.3 keV excitation energy is already known, but there is no spin assignment and the next member of this band has not previously been observed.

As can be seen from Fig. 4.17, this nucleus is not a usual rigid rotor. Due to insufficient available experimental information it is not possible to obtain firm spin assignments in the current work. Taking into account the calculations made by Roepke [Roe00] and the obtained transition scheme it is likely that the observed states are members of the 5/2 band with spins 5/2, 7/2, 9/2, 11/2 and 13/2. According to Fig. 4.17 it is likely that there are two bands which cross at 7/2 $\hbar$.

Moments of inertia

The moments of inertia extracted from the ground-state bands in ^{21,22,23}Ne are almost the same (see Table 4.3), which suggests similar structures. According to this the neon isotopes can be described as ^{20}Ne-core plus valence neutrons.

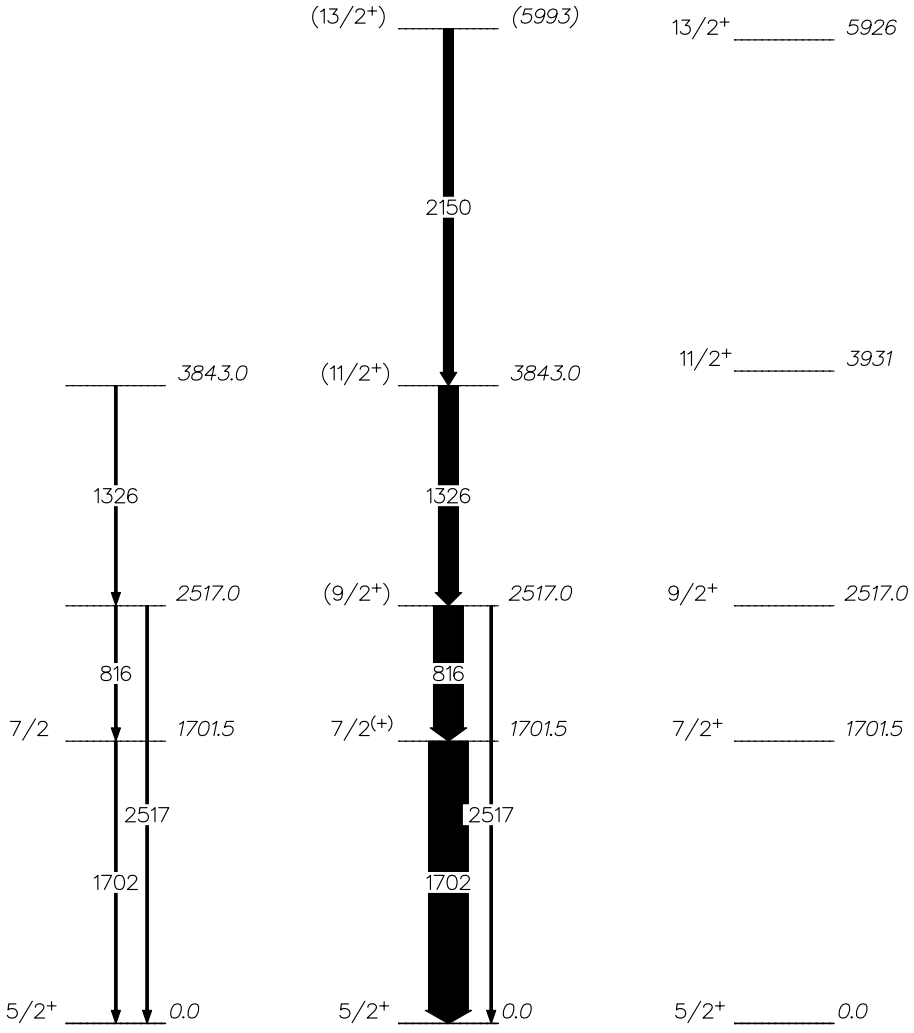

Figure 4.15: Gamma-ray decay scheme for ^{23}Ne as observed in this experiment (middle). On the left side of the picture is shown the previously known information about this nucleus and on the right side the predicted band calculated in Ref. [Roe00]. Energies are in keV. The widths of the arrows are only proportional to the relative intensities for the ground-state band. The widths of the arrows are proportional to the intensities for the current data (middle).

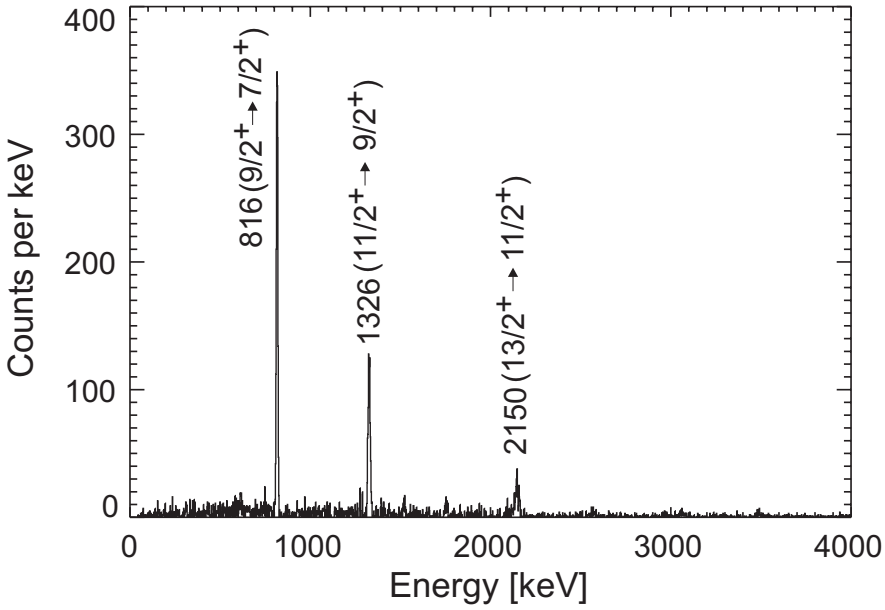

Figure 4.16: Gamma-decay spectrum gated by the ground state 1702 keV $(7/2^+ \rightarrow 5/2^+)$ transition of the $K^\pi = 5/2^+$, $T = 3/2$ band in ^{23}Ne.

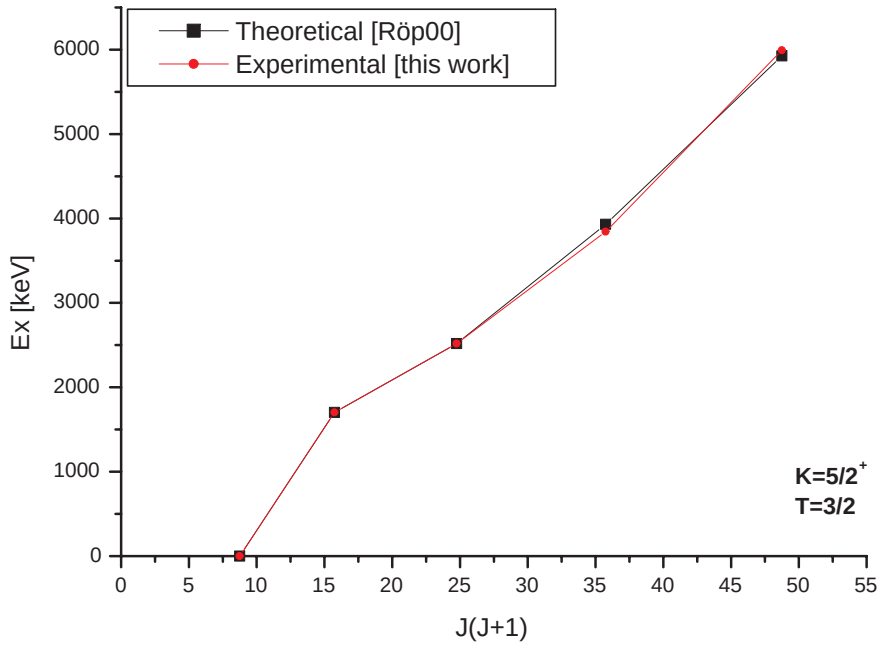

Figure 4.17: Excitation energy versus J(J+1) plot for the positive parity yrast band in ^{23}Ne as obtained from the current data.

Nucleus	Bandhead	α [keV]
^{21}Ne	$3/2^+$, $3/2^-$	145, 141
^{22}Ne	0^+	149
^{23}Ne	$5/2^+$	140

Table 4.3: Moments of inertia for the rotational bands in the neon isotopes.

4.4 Summary

The γ-ray decay of states populated in the ^{16}O(^{7}Li,2n) and ^{16}O(^{7}Li,np) reactions have been studied. The spectroscopy of ^{21}Ne has been extended with respect to the concept of reflection asymmetric shapes due to octupole deformation. Two parity doublets with $K = 3/2,\ 1/2$ were established. The mirror nucleus to ^{21}Ne, namely ^{21}Na, was investigated and the behaviour of the Coulomb energy difference (CED) was interpreted.

Furthermore, the γ-ray decay properties of ^{21,22,23}Ne, populated in the ^{18}O(^{13}C,xn) reaction, where x=0,1,2, have been studied. The decay scheme for the $K = 3/2$ band in ^{21}Ne suggests a 'pure' compound nucleus reaction in which mainly yrast states are populated.

New γ-ray transitions in ^{22}Ne and ^{23}Ne have been identified and the level schemes have been extended to higher spins. Possible spin assignments for the new transitions have been suggested. The results show good agreement with theoretical shell-model calculations performed by Roepke [Roe00].